AD-A090 195   VIRGINIA POLYTECHNIC INST AND STATE UNIV BLACKSBURG --ETC F/G 17/7
STAR PATTERN RECOGNITION AND SPACECRAFT ATTITUDE DETERMINATION.(U)
DEC 79 T E STRIKWERDA, J L JUNKINS DAAK70-78-C-0038

UNCLASSIFIED ETL-0211 NL

1 OF 1
AD
AD A090195

END
DATE
FILMED
11-80
DTIC

(12) F

ETL-0211 ✓

Ac80355

STAR PATTERN RECOGNITION AND SPACECRAFT ATTITUDE DETERMINATION

PHASE II

See 1473

Thomas E. Strikwerda
John L. Junkins

Engineering Science and Mechanics Department
Virginia Polytechnic Institute and State University
Blacksburg, Virginia 24061

December 1979

Interim Report for the period 1 October 1978 - 30 September 1979

Approved For Public Resease
Distribution Unlimited

Prepared for

U.S. Army Engineer Topographic Laboratories
Fort Belvoir, Virginia 22060

FORWARD

This document represents an interim report covering Phase II (FY79) of Contract DAAK70-78-C-0038 for the U.S. Army Engineer Topographic Laboratories, Fort Belvoir, Virginia.

The authors appreciate the capable guidance of Mr. L. A. Gambino, Director of the Computer Science Laboratory (USAETL), who served as Technical Monitor for this effort.

SUMMARY

The primary results of the Phase II efforts are the following:

1. Continued development and refinement of an approach for real time on-board estimation of spacecraft attitude with sub-five arc-second precision.

2. Implementation and validation of several variations of the approach in a laboratory microcomputer - the objective being to ascess the problems associated with a real-time, on-board version of this system.

3. Development of truth models to generate realistic input data for the star pattern recognition and Kalman filter strategies.

4. Conversion from use of Euler angles to Rodrigues parameters to define vehicle attitude, affecting the algorithms for star-pattern recognition, least-squares differential correction to refine estimated attitude, and the Kalman filter strategy to obtain the optimal attitude estimate.

5. Formulation of algorithms using Euler parameters to define orientation.

These results are discussed in detail herein.

TABLE OF CONTENTS

1.0 INTRODUCTION AND SYSTEM OVERVIEW

The purpose of the research activities described in this document is to research and develop a system for on-board attitude determination for satellites, achieving sub-five arc-second accuracy when such a system is interfaced with a general purpose star tracker (typical of several existing configurations).

The primary motivation for this research is the exploitation of recently developed light sensitive Charge-Doupled-Devices (CCD) in the focal plane of a tracker lens. The CCD will act as a "film" for imaging starlight and from which the attitude can be determined. The attitude determination can be performed on-board with a high degree of accuracy and high speed. A typical CCD for this application consists of about 200,000 light-sensitive elements or pixels, accurately imbedded (to 1 part in 10,000) in a microcircuit chip. The CCD can be scanned electronically and the voltage response of illuminated pixels digitized for processing by a microcomputer; corrections can be applied for image distortion based upon apriori calibration.

The image coordinate data, output by the computer, can be either telemetered to ground for later analysis or, as described in this report, analyzed on-board (via computers configured in parallel) to determine satellite attitude autonomously in near real-time.

The basic system we propose consists of 2 or 3 CCD star-trackers and 3 microcomputers, each with a dedicated function. The function of each of the 4 sub-systems is outlined below, with reference to Figures 1.1, 1.2 and 1.3.

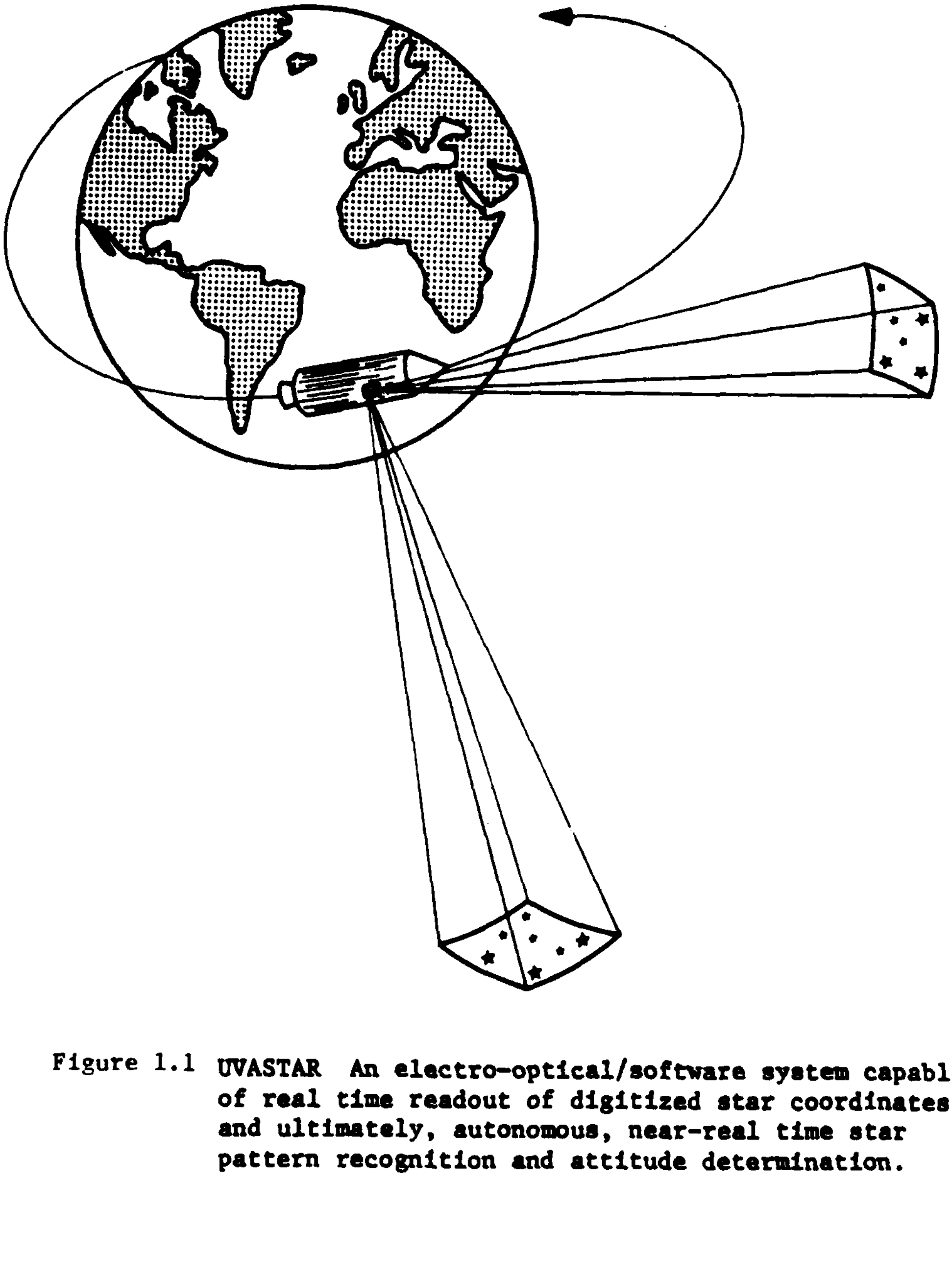

Figure 1.1 **UVASTAR An electro-optical/software system capable of real time readout of digitized star coordinates, and ultimately, autonomous, near-real time star pattern recognition and attitude determination.**

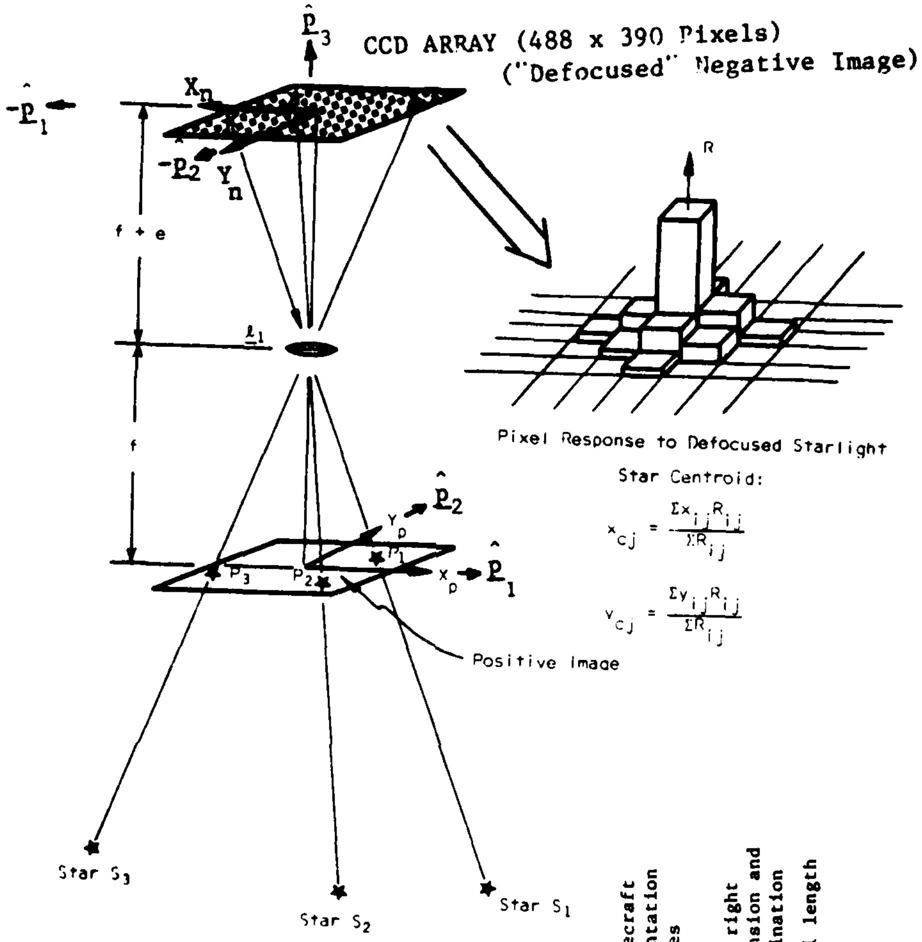

CCD ARRAY (488 x 390 Pixels)
("Defocused" Negative Image)
$\hat{p}_3$
$-\hat{p}_1$
X_n
$-\hat{p}_2$
Y_n
f + e
L_1
f
$\hat{p}_2$
Y_p
P_1
P_2
P_3
x_p
$\hat{p}_1$
Positive Image
R
Pixel Response to Defocused Starlight
Star Centroid:
$x_{cj} = \frac{\Sigma x_{ij} R_{ij}}{\Sigma R_{ij}}$
$y_{cj} = \frac{\Sigma y_{ij} R_{ij}}{\Sigma R_{ij}}$
Star S_3
Star S_2
Star S_1

Colinearity Equations:

$$X_n = f\left[\frac{C_{11}L_1 + C_{12}L_2 + C_{13}L_3}{C_{31}L_1 + C_{32}L_2 + C_{33}L_3}\right] = \text{function} \ (\overbrace{\phi,\ \theta,\ \psi}^{\text{Spacecraft Orientation Angles}},\ \overbrace{\alpha,\ \delta}^{\text{Star right Ascension and Declination}},\ \overset{\text{Focal length}}{f})$$

$$Y_n = f\left[\frac{C_{21}L_1 + C_{22}L_2 + C_{23}L_3}{C_{31}L_1 + C_{32}L_2 + C_{33}L_3}\right] = \text{function} \ (\phi,\ \theta,\ \psi,\ \alpha,\ \delta,\ f)$$

where

$$\left.\begin{array}{l} L_1 = \cos\delta\ \cos\alpha \\ L_2 = \cos\delta\ \sin\alpha \\ L_3 = \sin\delta \end{array}\right\} \text{star direction cosines,} \quad \left[C_{ij}\right] = \begin{bmatrix} \cos\psi & \sin\psi & 0 \\ -\sin\psi & \cos\psi & 0 \\ 0 & 0 & 1 \end{bmatrix} \begin{bmatrix} \cos\theta & 0 & -\sin\theta \\ 0 & 1 & 0 \\ \sin\theta & 0 & \cos\theta \end{bmatrix} \begin{bmatrix} 1 & 0 & 0 \\ 0 & \cos\phi & \sin\phi \\ 0 & -\sin\phi & \cos\phi \end{bmatrix}$$

Figure 1.2 Formation of Image on the CCD Array.

Figure 1.3

STAR PATTERN RECOGNITION/SPACECRAFT ATTITUDE ESTIMATION

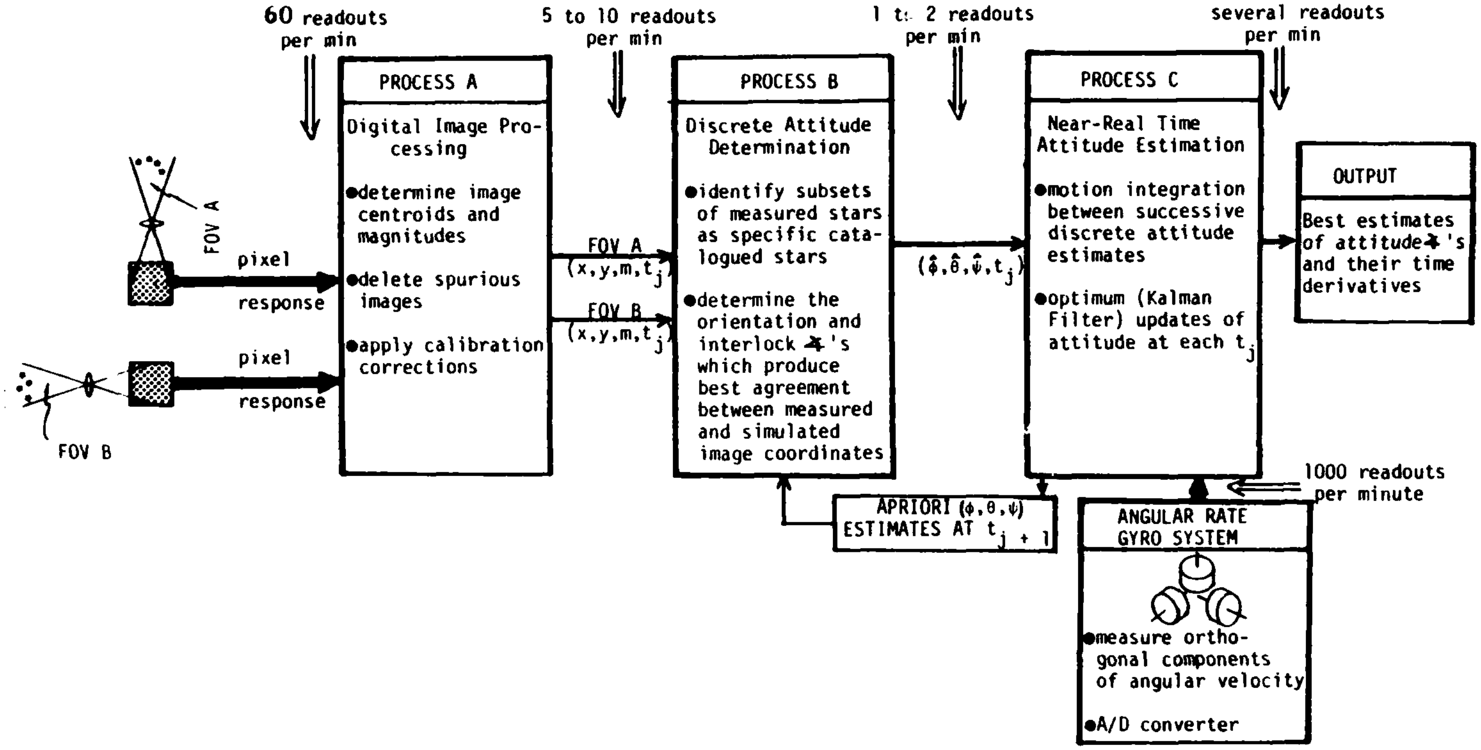
60 readouts per min
5 to 10 readouts per min
1 t: 2 readouts per min
several readouts per min
FOV A
FOV B
pixel response
pixel response
PROCESS A
Digital Image Processing
●determine image centroids and magnitudes
●delete spurious images
●apply calibration corrections
FOV A (x,y,m,t_j)
FOV B (x,y,m,t_j)
PROCESS B
Discrete Attitude Determination
●identify subsets of measured stars as specific catalogued stars
●determine the orientation and interlock ∢'s which produce best agreement between measured and simulated image coordinates
($\hat{\phi}, \hat{\theta}, \hat{\psi}, t_j$)
PROCESS C
Near-Real Time Attitude Estimation
●motion integration between successive discrete attitude estimates
●optimum (Kalman Filter) updates of attitude at each t_j
OUTPUT
Best estimates of attitude∢'s and their time derivatives
APRIORI (ϕ, θ, ψ) ESTIMATES AT t_{j+1}
1000 readouts per minute
ANGULAR RATE GYRO SYSTEM
●measure orthogonal components of angular velocity
●A/D converter

1) CCD State Sensors and Associated Electronics.

Although the development of CCD sensors and CCD trackers is not part of this research, there are several CCD star tracker designs proposed by various organizations involved in hardware development. The purpose of our work has been exploitation of the CCD star tracker technology; we have chosen a particular set of parameters but it should be kept in mind that these are nominal, achievable values without further CCD/star tracker technology advances. Each of the two (or three) trackers (assumed in various configurations herein) is identical and their boresights are assumed separated by the nominal interlock angle of 90°. We assume a lens focal length of 70 mm and a CCD array size such that a 7° x 9° field of view (FOV) is imaged onto the array. The arrays are assumed to be Fairchild's 11.4 mm x 8.8 mm matrix consisting of 488 x 380 silicon pixels. Starlight is defocused slightly on the CCD in order to spread typical images over 9 to 25 adjacent pixels. This permits accurate "centroiding" of the image to determine image coordinates accurate to about 10% of a pixel. The processing of a data frame consists of a rapid analog readout of all pixels and an analog to digital (A/D) conversion only of selected pixels (based upon response above an analog threshold level). The scans of each field of view are controlled by a common clock and are assumed to represent 2 (or 3) frames (1 from each sensor) taken at the same instant. This assumption is valid for all but very rapidly spinning satellites, since the CCDs can be scanned 10 times per second.

2) Microcomputer A

Program Process A is performed by Microcomputer A with either one computer per sensor or sequential treatment of data for 2 or 3 sensors. Again, Process A is not part of this research program. Since the functions to be performed are straightforward, we simply replace Process A by calculating synthetic output data whose availiability is clock controlled. Process A takes as input data the digitized pixel voltages and pixel coordinates for up to 6 stars in each FOV and the associated time. Image centroids are calculated for each image and corrections for lens distortion and other known error sources are applied and a relative magnitude or intensity is calculated. The output of Process A consists of the focal plane coordinates for each star image. Since Process A calculations for one data frame can be performed in near real time and many times faster than the attitude can be determined, it will likely prove desirable to perform additional editing of the star data. For example, images with rapidly varying image intensity from frame to frame could be eliminated or images whose successive positions are inconsistent with the overall motion caused by vehicle motion (such as images of space debris) could be deleted immediately from consideration (failure to detect and delete all spurious images does not prove fatal, but does slow the pattern recognition logic of Process B). Process A would be expected to output image coordinate and magnitude data at the rate of about 5 frames per sensor each minute and simply overwrite old data.

The microcomputer of Process A is considered as an integral part of the star tracker itself, making it a "smart sensor".

Since Process A controls the scan of the CCD and its electronics, it is possible to track only those stars desired (those whose pixel response lies within specified bounds). Thus, even though the CCD array contains thousands of pixels, only a small fraction of their response values need be subjected to A/D conversion and stored at any one time. It is this data compaction feature, along with the fact that pixel locations can be accurately calibrated, that make CCD arrays so attractive for this application. Also significant is that the high speed readout of the CCD allows one to assume, for most cases, that the star images visible in a given frame have been imaged simultaneously. It is therefore possible to use stellar resection (geometric) methods and not necessary to account for the vehicle motion between successive "hits" within a single frame of data.

3) Microcomputer B

Data from Process A (and Process C) are analyzed by program *Process B*; again by means of a dedicated microcomputer. As input, Process B accepts:

* star image coordinates and magnitude data; one set per FOV (from Process A),
* a priori attitude estimates and covariance, (from Process C), and
* a priori estimates and covariance of interlock angles between the sensors image planes (from Process C).

The sequence of calculations/logical decisions divides into two primary functions:

* identify measured stars in each FOV as specific stars contained in an on-board star catalog (containing, in the general case, the direction cosines and instrument magnitudes of the 5000 brightest stars) and
* determine the spacecraft orientation and field of view interlock angles which cause the simulated images of identified catalog stars to overlay the corresponding measured images in a least-squares sense.

These two tasks will be discussed in detail in Sections 2.1 and 5.1. The expected output rate for Process B is two or more attitude updates per minute of elapsed time. The old attitude and covariance is overwritten by each new attitude and covariance and the new values are output to Process C.

4) Microcomputer C

The attitude determined by Process B for a discrete time is further processed by program Process C in microcomputer C. Input to this program consists of the attitude and covariance from Process B and A/D converted gyro rate measurements of angular velocity. The previous orientation estimates are integrated forward (using the gyro rate measurements) to the time associated with the new orientation from Process B. The two orientations are combined in a Kalman Filter calculation to give a best estimate of real-time attitude. Further forward integration gives an estimated orientation and covariance for the next Process B input.

During Phase II of this project our efforts have been primarily in the following areas:

1) Conversion from Euler angles to Rodrigues parameters to describe the spacecraft orientation (affecting the algorithms of Processes B and C).
2) Improvements in the efficiency of Processes B and C calculations and adding several needed refinements.
3) Formulation of a "truth model" for adequately testing Processes B and C.
4) Design of an efficient star catalog format for easy access.
5) Develop the formulation for conversion from Rodrigues parameters to Euler parameters for satellite attitude in both Processes B and C.

These and other topics are discussed in this report. All our work involving computer software during Phase II has been performed using the HP9845A microcomputer system. We also discuss herein the anticipated continuation of the above work and new tasks, to be carried out during Phase III of the project.

2.0 ORIENTATION PARAMETERS

The Phase I report outlined the Process B calculations needed to determine the vehicle orientation from the star image coordinates. The solution equations involved a set of three Euler angles defining the rotation sequence for orienting the field of view (FOV) relative to inertial space. Any 3 angle set leads to differential equations and estimation algorithms containing two geometric singularities ($\phi = \pm \pi/2$ for the 1-2-3 ω-ϕ-κ sequence.) Also, Euler angles are invariably governed by equations having trigonometric nonlinearities; this increases the expense of numerical integration. A significant change in Process B since the Phase I report has been the introduction of Rodrigues parameters as a set of 3 parameters defining the FOV orientation. The Euler-Rodrigues parameters have only one singular orientation and they are governed by equations having quadratic nonlinearities. During Phase III of this project we will explore the use of Euler parameters to define FOV orientation. The four Euler parameters have the advantages that (1) they do not have a geometric singularity, and (2) they rigorously satisfy linear differential equations. The presence of the constraint that they sum square to unity causes some problems in estimation algorithms; however, we recently found a method to circumvent this difficulty. Since Rodrigues parameters are most easily derived from Euler parameters, we shall describe the latter parameter set first.

2.1 Euler Parameters

Euler parameters ($\beta_0, \beta_1, \beta_2, \beta_3$) can be interpreted geometrically in terms of Euler's theorem: "A completely general angular displacement of a rigid body can be accomplished by a single rotation (the <u>principal</u>

angle, ϕ) about a line (the principal line, $\hat{\ell}$) which is fixed relative to both arbitrary body-fixed axes $\{\hat{b}\}$ and reference axes $\{\hat{n}\}$. If $\{\hat{n}\}$ is initially coincident with $\{\hat{b}\}$, then the direction cosines (ℓ_1,ℓ_2,ℓ_3) of $\hat{\ell}$ with respect to $\{\hat{n}\}$ and $\{\hat{b}\}$ are identical."

The Euler parameters are then related to the principal rotation parameters as follows:

$$\begin{aligned} \beta_0 &= \cos \phi/2 \\ \beta_i &= \ell_i \sin \phi/2 \quad , \quad i=1,2,3. \end{aligned} \tag{2.1}$$

Note that Euler parameter satisfy the constraint:

$$\sum_{i=0}^{3} \beta_i^2 = 1. \tag{2.2}$$

The rotation matrix [C] characterizing the relationship between a body fixed frame $\{\hat{b}\}$ and a reference frame $\{\hat{n}\}$ by: $\{\hat{b}\} = [C]\{\hat{n}\}$ can be written in terms of Euler parameters as:

$$[C] = \begin{bmatrix} \beta_0^2 + \beta_1^2 - \beta_2^2 - \beta_3^2 & 2(\beta_1\beta_2 + \beta_0\beta_3) & 2(\beta_1\beta_3 - \beta_0\beta_2) \\ 2(\beta_1\beta_2 - \beta_0\beta_3) & \beta_0^2 - \beta_1^2 + \beta_2^2 - \beta_3^2 & 2(\beta_2\beta_3 + \beta_0\beta_1) \\ 2(\beta_1\beta_3 + \beta_0\beta_2) & 2(\beta_2\beta_3 - \beta_0\beta_1) & \beta_0^2 - \beta_1^2 - \beta_2^2 + \beta_3^2 \end{bmatrix} \tag{2.3}$$

The two main advantages of Euler parameters are that (1) no singularity exists for any orientation, and (2) no evaluation of trignometric functions need be done. The constraint (2.2), must be carefully accounted for, however.

We intend to explore the use of Euler parameters for both Process B and C during Phase III. From preliminary analysis it appears Process B can be adapted easily to Euler parameters. The only disadvantage in using Euler parameters is the need for a constraint equation in performing the least-squares correction. We outline two methods we have tried for incorporating this constraint equation in Process B.

In Process B we seek to minimize the sum of the squares of the residuals between measured star image coordinates and predicted coordinates for the same stars, using direction cosines from the on-board catalog. The mapping of catalog positions onto the CCD image plane is a function of the orientation parameters (Euler angles, Euler parameters, or Rodrigues parameters) via the stellar colinearity equations:

$$x = f\left\{\frac{AN_{11}L_1 + AN_{12}L_2 + AN_{13}L_3}{AN_{31}L_1 + AN_{32}L_2 + AN_{33}L_3}\right\}$$

$$y = f\left\{\frac{AN_{21}L_1 + AN_{22}L_2 + AN_{23}L_3}{AN_{31}L_1 + AN_{32}L_2 + AN_{33}L_3}\right\} \qquad (2.4)$$

where f = lens focal length

AN_{ij} = elements of the coordinate frame rotation matrix [AN].

L_i = star direction cosines.

If we let:

$X = \{(x_i,y_i)\}$ = vector of <u>calculated</u> CCD image plane coordinates.

$\tilde{X} = \{(x_i,y_i)\}_m$ = vector of <u>measured</u> star image positions on the CCD.

and $\Delta X = \tilde{X} - X$ = vector of residuals,

then we seek to find the set of Euler parameters, ß, such that the weighted sum of the squares of the residuals is minimized; i.e., minimize

$$\phi = \Delta X^T W \Delta X \qquad (2.5)$$

It can be shown that minimizing the function ϕ can be achieved by minimizing a function ϕ_p iteratively;;

$$\phi_p = \Delta X_p^T W \Delta X_p \qquad (2.6)$$

where $\Delta X_p = \tilde{X} - X_p$ and

X_p = vector of linearly predicted image coordinates.

But, by first-order Taylor expansion

$$\Delta X_p = \Delta X_c - A\ \Delta\beta$$

where

ΔX_c = vector of current image coordinates residuals based current estimates of β.

A = matrix of partial derivatives of the colinearity equations with respect to Euler parameters

$\Delta\beta$ = corrections to the current estimates of Euler parameters.

Thus, we can write:

$$\phi_p = (\Delta X_c - A\Delta\beta)^T\ W(\Delta X_c - A\Delta\beta). \tag{2.7}$$

In addition to finding the set of Euler parameters to minimize ϕ_p, we must also satisfy the constraint equation:

$$\beta^T\beta = 1. \tag{2.8}$$

Letting $\beta_p = \beta_c + \Delta\beta$, we find:

$$(\beta_c + \Delta\beta)^T\ (\beta_c + \Delta\beta) = 1$$

or to first order:

$$1 - \beta_c^T\beta_c = 2\beta_c^T\Delta\beta. \tag{2.9}$$

Thus, our problem requires that we minimize Eq. 2.7 subject to the constraint equation, Eq. 2.9. To obtain the corrections we minimize the augmented function, Φ, using the method of Lagrange multipliers:

$$\Phi = (\Delta X_c - A\Delta\beta)^T\ W(\Delta X_c - A\Delta\beta) + \lambda(2\Delta Y - 2\beta^T\Delta\beta) \tag{2.10}$$

where $\Delta Y = (1 - \beta^T\beta)/2$

λ = a scalar Lagrange multiplier.

For minimization, we require:

$$\nabla_{\Delta\beta}\Phi = -2A^TW\Delta X_c + 2(A^TWA)\Delta\beta - 2\lambda\beta = 0 \tag{2.11}$$

and

$$\nabla_\lambda \Phi = 2\Delta Y - 2\beta^T = 0 \quad \text{or}$$

$$\Delta Y = \beta^T \Delta\beta. \tag{2.12}$$

We combine these two equations as follows. Solve Eq. 2.11 for $\Delta\beta$:

$$\Delta\beta = (A^T WA)^{-1} A^T W \Delta X_c + (A^T WA)^{-1} \beta\lambda \tag{2.13}$$

Substitute this into equation 2.12:

$$\Delta Y = \beta^T (A^T WA)^{-1} A^T W \Delta X_c + \beta^T (A^T WA)^{-1} \beta\lambda. \tag{2.14}$$

Solve for λ:

$$\lambda = (\beta^T (A^T WA)^{-1} \beta)^{-1} (\Delta Y - \beta^T (A^T WA)^{-1} A^T W \Delta X_c). \tag{2.15}$$

Finally, substitute for λ in Eq. 2.13 to eliminate λ. We prefer to write this final equation as:

$$\hat{\Delta\beta} = \Delta\bar{\beta} + K(\Delta Y - \beta^T \Delta\bar{\beta}) \tag{2.16}$$

where $\Delta\bar{\beta} = (A^T WA)^{-1} A^T W \Delta X_c$

= corrections to β without the constraint and

$$K = (A^T WA)^{-1} \beta (\beta^T (A^T WA)^{-1} \beta)^{-1}.$$

Unfortunately, Eq. 2.16 does not work well for our application, although the general formulation is useful in other applications. Matrix $A^T WA$ appears to be singular or very nearly so and thus, in the present application, $(A^T WA)^{-1}$ can not be determined (matrix A "knows" that there are really only 3 degrees of freedom!).

Therefore, we have tried an alternate, and, in the limit, equivalent, solution for $\Delta\beta$. The constraint equation can be incorporated as an additional "perfect" observation equation but with a large weight. That is, $\Delta Y = (1 - \beta^T \beta)/2$ is appended to the ΔX_c vector of equation (2.7) and β^T appended as an additional row in to the A matrix of equation (2.7). The weight for this equation, the (4,4) element of W, is chosen large enough (about 10^6) so that $(A^T WA)^{-1}$ does not change appreciably for variations in this weight. The solution for $\Delta\beta$ is then the classical normal equations:

$$\Delta\beta = (A^T W A)^{-1} A^T W \Delta X_c \tag{2.17}$$

This solution for $\Delta\beta$ has been found to be stable for all cases we have tried and is more convenient than equation (2.16) (which is, by the way, simply thé Kalman Filter algorithm particularized to the present case of a perfect measurement having infinite weight or zero variance).

The use of Euler parameters in Process C should be a straightforward modification of the present software, which involves Rodrigues parameters. In addition, there are several properties of Euler parameters which will be utilized to advantage.

We have decided, for the present formulation, to use a seven parameter state vector for Process C. This consists of the four Euler parameters $\{\beta_i(t)\}$ and three unknown, slowly varying, rate gyro biases, one per gyro. The biases will absorb unmodeled errors such as gyro nonorthogonality, gyro interlocks, etc. (Rigorous justification for including only the rate biases is difficult, so we shall do simulations). We assume that the biases are constant over several minutes and we then monitor their values over longer periods.

The Euler parameter differential equations describing the rotational kinematics of a space vehicle are:

$$\begin{Bmatrix} \dot\beta_0 \\ \dot\beta_1 \\ \dot\beta_2 \\ \dot\beta_3 \end{Bmatrix} = \frac{1}{2} \begin{bmatrix} \beta_0 & -\beta_1 & -\beta_2 & \beta_3 \\ \beta_1 & \beta_0 & -\beta_3 & \beta_2 \\ \beta_2 & \beta_3 & \beta_0 & -\beta_1 \\ \beta_3 & -\beta_2 & \beta_1 & \beta_0 \end{bmatrix} \begin{Bmatrix} 0 \\ \omega_1 \\ \omega_2 \\ \omega_3 \end{Bmatrix} = [\omega(t)] \begin{Bmatrix} \beta_0 \\ \beta_1 \\ \beta_2 \\ \beta_3 \end{Bmatrix} \tag{2.18}$$

$$\text{where } [\omega(t)] = \frac{1}{2}\begin{bmatrix} 0 & -\omega_1 & -\omega_2 & -\omega_3 \\ \omega_1 & 0 & \omega_3 & -\omega_2 \\ \omega_2 & -\omega_3 & 0 & \omega_1 \\ \omega_3 & \omega_2 & -\omega_1 & 0 \end{bmatrix}$$

where $\{\omega_i\}$ are the rate gyro readout values (including noise) for vehicle rotation with components along the 3 orthogonal gyro frame axes. Since the biases are assumed constant over short time intervals their differential equations are:

$$\left\{\begin{matrix} \dot{b}_1 \\ \dot{b}_2 \\ \dot{b}_3 \end{matrix}\right\} = 0. \qquad (2.19)$$

This set of seven equations is integrated forward in time using 4-cycle Runge-Kutta methods. The values of $\{\beta_i(t)\}$ are then passed to Process B to be used for the analysis of the next frame.

In addition to this set of equations, we must also obtain the (7×7) state transition matrix, $\Phi(t,t_k)$, for the Kalman filter state update equations:

$$[\Phi(t,t_k)] = \left[\frac{\partial(\beta_0(t),\ \beta_1(t),\ \beta_2(t),\ \beta_3(t),\ b_1(t),\ b_2(t)\ b_3(t))}{\partial(\beta_0(t_k),\ \beta_1(t_k),\ \beta_2(t_k),\ \beta_3(t_k),\ b_2(t_k),\ b_3(t_k))}\right]$$

$$= \left[\begin{array}{c|c} \Phi_{11} & \Phi_{12} \\ \hline 0 & I \end{array}\right] \qquad (2.20)$$

The upper left 4×4 portion, Φ_{11}, of Φ can be found from integration of:

$$\left[\frac{d\Phi_{11}(t,t_k)}{dt}\right] = [\omega(t)]\ [\Phi_{11}(t,t_k)]\ . \qquad (2.21)$$

and Φ_{11} satisfies:

$$\{\beta(t)\} = [\Phi_{11}(t,t_k)]\{\beta(t_k)\} \quad , \quad \Phi_{11}(t_k,t_k) = [I]. \tag{2.23}$$

However, detailed analysis of the 16 differential equations comprising Eq. 2.2 reveals that there are only 4 distinct equations for elements ϕ_{ij} of Φ_{11}:

$$\Phi_{11}(t,t_k) = \begin{bmatrix} \phi_{11} & \phi_{12} & \phi_{13} & \phi_{14} \\ -\phi_{12} & \phi_{11} & -\phi_{14} & \phi_{13} \\ -\phi_{13} & \phi_{14} & \phi_{11} & -\phi_{12} \\ -\phi_{14} & -\phi_{13} & \phi_{12} & \phi_{11} \end{bmatrix} . \tag{2.24}$$

Equation 2.23 becomes, then,

$$\begin{Bmatrix} \beta_0(t) \\ \beta_1(t) \\ \beta_2(t) \\ \beta_3(t) \end{Bmatrix} = \begin{bmatrix} \phi_{11} & \phi_{12} & \phi_{13} & \phi_{14} \\ -\phi_{12} & \phi_{11} & -\phi_{14} & \phi_{13} \\ -\phi_{13} & \phi_{14} & \phi_{11} & -\phi_{12} \\ -\phi_{14} & -\phi_{13} & \phi_{12} & \phi_{11} \end{bmatrix} \begin{Bmatrix} \beta_0(t_k) \\ \beta_1(t_k) \\ \beta_2(t_k) \\ \beta_3(t_k) \end{Bmatrix}$$

this can be rearranged ("transmuted") to:

$$\begin{Bmatrix} \beta_0(t) \\ \beta_1(t) \\ \beta_2(t) \\ \beta_3(t) \end{Bmatrix} = \begin{bmatrix} \beta_0(t_k) & \beta_1(t_k) & \beta_2(t_k) & \beta_3(t_k) \\ \beta_1(t_k) & -\beta_0(t_k) & \beta_3(t_k) & -\beta_2(t_k) \\ \beta_2(t_k) & -\beta_3(t_k) & -\beta_0(t_k) & \beta_1(t_k) \\ \beta_3(t_k) & \beta_2(t_k) & -\beta_1(t_k) & -\beta_0(t_k) \end{bmatrix} \begin{Bmatrix} \phi_{11} \\ \phi_{12} \\ \phi_{13} \\ \phi_{14} \end{Bmatrix} . \tag{2.25}$$

By noticing that the coefficient matrix above is orthogonal we can write its inverse as simply:

$$\begin{Bmatrix} \Phi_{11} \\ \Phi_{12} \\ \Phi_{13} \\ \Phi_{14} \end{Bmatrix} = \begin{bmatrix} \beta_0(t_k) & \beta_1(t_k) & \beta_2(t_k) & \beta_3(t_k) \\ \beta_1(t_k) & -\beta_0(t_k) & -\beta_3(t_k) & \beta_2(t_k) \\ \beta_2(t_k) & \beta_3(t_k) & -\beta_0(t_k) & -\beta_1(t_k) \\ \beta_3(t_k) & -\beta_2(t_k) & \beta_1(t_k) & -\beta_0(t_k) \end{bmatrix} \begin{Bmatrix} \beta_0(t) \\ \beta_1(t) \\ \beta_2(t) \\ \beta_3(t) \end{Bmatrix} . \tag{2.26}$$

Thus, the elements of $\Phi_{11}(t,t_k)$ can be obtained from the values of $\{\beta_i(t_k)\}$ and $\{\beta_i(t)\}$ rather than from integration of the original 16 equations of Φ_{11}. This property will be used to advantage to reduce the number of calculations in Process C.

The 4×3 matrix Φ_{12} must be formed by direct integration of

$$\left[\frac{d\Phi_{12}(t,t_k)}{dt}\right] = [\omega(t)][\Phi_{12}(t,t_k)] + [A_{12}] \tag{2.27}$$

where

$$[A_{12}] = \left[\frac{\partial(\dot{\beta}_0(t),\ \dot{\beta}_1(t),\ \dot{\beta}_2(t),\ \dot{\beta}_3(t))}{\partial(b_1,\ b_2,\ b_3)}\right] \tag{2.28}$$

$$[\Phi_{12}(t_k,t_k)] = 0.$$

<u>Kalman</u> <u>Filter</u> <u>Section</u> <u>of</u> <u>Process</u> <u>C</u>.

The state covariance and Kalman gain update recursions are the same forms used in the Phase I report:

$$\hat{X}_{k+1} = \overline{X}_k(k+1) + K(k+1)\{\tilde{Y}(k+1) - \overline{Y}(k+1)\}$$

$$P_k(k+1) = \Phi(k+1,k)\ P_k(k)\Phi^T(k+1,k) + Q(k)$$

$$K_{(k+1)} = P_k(k+1)H^T(k+1)[\Lambda_{v_{k+1}v_{k+1}} + H(k+1)P_k(k+1)H^T(k+1)]^{-1} \tag{2.29}$$

$$P_{k+1}(k+1) = [I - K(k+1)H(k+1)]P_k(k+1)$$

$$H(k+1) = \frac{\partial Y}{\partial X}\bigg|_{\overline{X}_k(k+1)}$$

where $\overline{X}_k(k+1)$ = state X at time t_{k+1} based upon k data subsets

= forward Runge-Kutta integration of equations 2.18 and 2.19 from the previous estimates $\hat{X}_k(k)$,

$$\overline{Y}(k+1) = \left\{ \begin{matrix} \beta_0(t_{k+1}) \\ \beta_1(t_{k+1}) \\ \beta_2(t_{k+1}) \\ \beta_3(t_{k+1}) \end{matrix} \right\} = \text{first four elements of } \overline{X}_k(k+1),$$

$\tilde{Y}(k+1)$ = values of $\{\beta(t_{k+1})\}$ from Process B, and

$Q(t)$ = process noise covariance matrix to reflect uncertainty in $(\beta_0, \beta_1, \beta_2, \beta_3)$ arising due to integration of errors in the rate gyro measurements.

2.2 Rodrigues Parameters

In constrast to Euler parameters, Rodrigues parameters form a three parameter set, thereby eliminating the need for a constraint equation. However, the Rodrigues parameters have a singularity like Euler angles (although any Euler angle set has two!). Computationally they are attractive since they, too, do not involve evaluation of trignometric functions for either the least-squares correction of Process B nor the Runge-Kutta integration of Process C.

Rodrigues parameters, $\{q_i\}$ are related to Euler parameters $\{\beta_i\}$ by:

$$q_i = \beta_i/\beta_o = \ell_i \tan \Phi/2 \quad , \quad i=1,2,3 \qquad (2.30)$$

The singularity occurs at $\Phi = 180°$. The 3×3 matrix for coordinate frame rotation, [C], expressed in Rodrigues parameters is:

$$[C] = \frac{1}{1+\sum q_i^2}\begin{bmatrix} 1 + q_1^2 - q_2^2 - q_3^2 & 2(q_1q_2 + q_3) & 2(q_1q_3 - q_2) \\ 2(q_1q_2 - q_3) & 1 - q_1^2 + q_2^2 - q_3^2 & 2(q_2q_3 + q_1) \\ 2(q_1q_3 + q_2) & 2(q_2q_3 - q_1) & 1 - q_1^2 - q_2^2 + q_3^2 \end{bmatrix} \quad (2.31)$$

and the kinematic equations are:

$$\begin{Bmatrix} \dot{q}_1 \\ \dot{q}_2 \\ \dot{q}_3 \end{Bmatrix} = \frac{1}{2}\begin{bmatrix} 1 + q_1^2 & q_1q_2 - q_3 & q_1q_3 + q_2 \\ q_1q_2 + q_3 & 1 + q_2^2 & q_2q_3 - q_1 \\ q_1q_3 - q_2 & q_2q_3 + q_1 & 1 + q_3^2 \end{bmatrix}\begin{Bmatrix} \omega_1 \\ \omega_2 \\ \omega_3 \end{Bmatrix} \quad (2.32)$$

Process B and C are currently operational using these parameters.

The simulations described in this report have all been performed using the Rodrigues parameters. Process B and C equations are very similar to the development reported in section 2.1 except for 3 parameters instead of 4. The tradeoffs between Euler parameters and Rodrigues parameters are the following:

(1) The Euler parameters are universal; no geometric singularity exicts, whereas the Rodrigues parameters still possess a singular point.

(2) The Euler parameters' state transition matrix can be found without numerical integration [see Eqs. (2.21) - (2.26)], whereas these developments do not hold for Rodrigues parameters.

(3) The three Rodrigues parameters result in lower dimensional matrices to invert than the four Euler parameters, in Process B calculations.

Advantages (1) and (2) outweigh, in our judgement, disadvantage (3) of the

Euler parameters in comparison to Rodrigues parameters. It is also significant to note that both Euler parameters or Rodrigues parameters are computationally superior to Eulerian angles, since no trigonometric nonlinearities are present in the differential equations.

3.0 COORDINATE FRAMES

We have used several coordinate frames thus far for the development of Process B and C algorithms. Refer to the Phase I Report for a complete discussion of possible frames and their interrelationships.

The two FOV frames used for the research described here are assumed to be separated by 90° and their orientations are nominally fixed relative to the vehicle gyro axes. The gyro frame unit vectors, $\{\underline{g}_i\}$, are assumed oriented such that $\underline{g}_1$ is along the vehicle x-axis (pointing in the direction of flight) and $\underline{g}_2$ and $\underline{g}_3$ are perpendicular to the vehicle x-axis. The FOV(A) frame orientation can be described by a (1,2,3) Euler angle sequence of (90°, 135°, 0°) relative to the gyro frame. This sequence places $\underline{a}_2$ (the image plane "y" axis) along $\underline{g}_3$ and $\underline{a}_3$ (the boresight) rotated 45° from $\underline{g}_1$ about $\underline{g}_3$. The FOV(B) frame is oriented relative to FOV(A) by a (3,1,3) Euler angle sequence of (90°, -90°, 90°). Again, $\underline{b}_2$ lies along $\underline{g}_3$ and $\underline{b}_3$ (the boresight) is rotated 45° from $\underline{g}_1$ about $\underline{g}_3$ (see Figure 3.1).

The gyro frame to FOV(A) and (B) rotations described above have been used for generating simulated data for Process B (see Chapter 4). The gyro frame is oriented such that $\underline{g}_2$ is perpendicular to the orbit plane and $\underline{g}_3$ along the radius vector. In Process B we do not use the gyro frame. Rather, the algorithms have been written to solve for the orientation parameters relating FOV(A) and (B) to the inertial frame.

We have not pursued the use of an orbiting frame as suggested in the Phase I report. The expected conversion to Euler parameters will obviate the need for defining the vehicle orientation relative to an orbiting frame because Euler parameters contain no inherent singularity as do Euler angles and Rodrigues parameters. Thus, by using Euler parameters, the dynamic and kinematic algorithms developed as part of this project will be applicable to any spacecraft and not be dependent on choice of a suitable orbiting frame to avoid singularities for each type of mission.

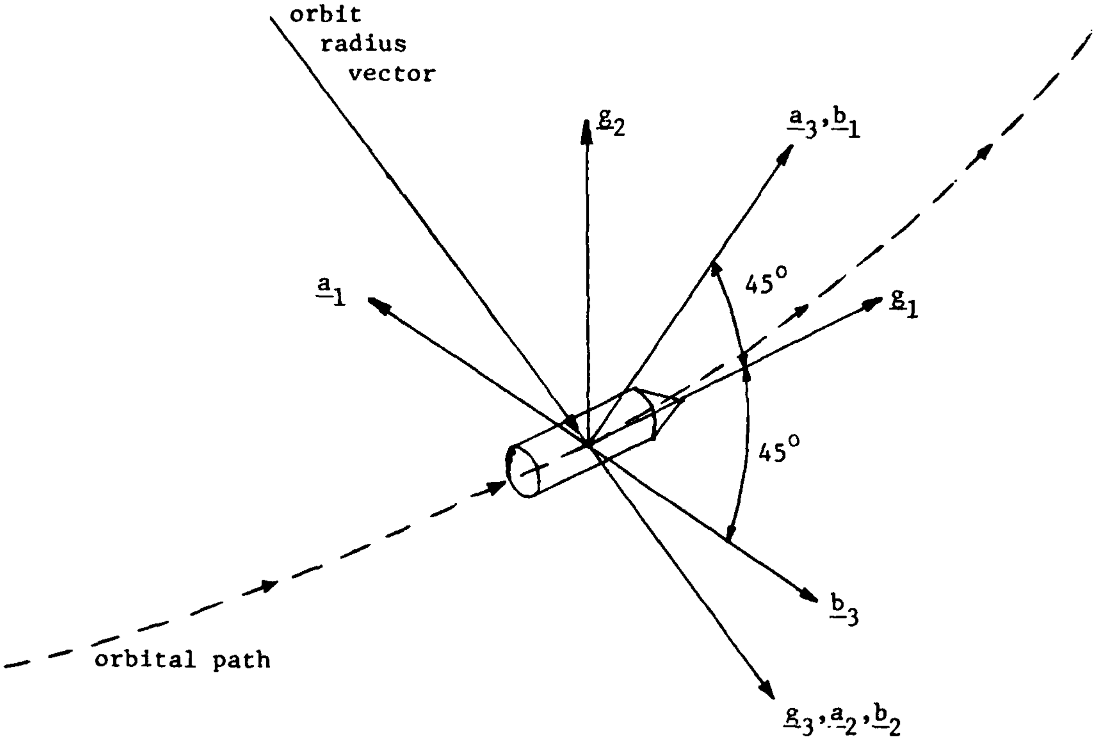

Figure 3.1. Relationship of the gyro frame to FOV(A) and FOV(B)

4.0 TRUTH MODELS

4.1 Process B Models

In order to adequately test Process B we must generate realistic input data (i.e., realistic output data from Process A). This requires generating a sequence of data frames using an assumed vehicle orbit and appropriate time intervals between successive frames. The image coordinates must be perturbed by relevant noise sources, and occasional additions of spurious images as well.

The first step in the data generation is to choose an appropriate spacecraft orbit by selecting the semi-major axis of the orbit, orbital period and initial position in inertial space. To facilitate the calculation of subsequent satellite positions we make use of Herrick's "f and g" solution (see Junkins, p. 155). This method is used also for computing the position and velocity of the earth at subsequent times.

Tests to date have been for a nearly circular orbit using a nominally earth pointing spacecraft. The nominal gyro frame orientation is then determined from the vehicle velocity and coordinate vectors. Thus, $\underline{g}_1$ is along $\underline{v}$, $\underline{g}_2$ is perpendicular to the orbit plane and $\underline{g}_3$ will be defined by the cross product of $\underline{g}_1$ and $\underline{g}_2$. The FOV(A) and (B) frames are then defined relative to $\{\underline{g}\}$ as described in section 3.

Given the boresight of each FOV, the star catalog is accessed in the same manner as in Process B (see Appendix A and the Phase I report). The combined velocity of the earth and vehicle is used to compute the aberration of starlight for each star (see Appendix B). The resulting star direction cosines are then rotated into the FOV and the image plane coordinates are computed using the colinearity equations and an assumed lens focal length of 70mm + ε, where ε is a small defocusing length needed to blur the star-image enough to allow accurate centroiding. For our purpose, we have assumed that the centroiding can be performed to an accuracy of better than 10% of a pixel and corrections to image location can be applied for causes such as image distortions. Thus, we add random Gaussian noise (with $\sigma \cong 3.4\mu$) to the image coordinates of each star to simulate centroiding errors. Star magnitudes are obtained from the star catalogue and are perturbed with noise also.

The true orientation and image coordinates as well as the error-corrupted simulated data are stored on computer tape. At present, we separate data frames by 30 seconds of satellite motion since that is the time needed for Process B solution. Upon application of the pattern recognition and estimation algorithms, all orientation parameters, interlock parameters, etc., can be compared versus the stored truth model.

4.2 Process C Models

For our tests of Process C we generated data for a series of satellite positions, again separated by 30 seconds of real time. The data consists of true orientation parameters and perturbed values representing output from Process B and an associated covariance matrix which would result from the least-squares solution. Eventually, we will use the actual output from Process B as input to Process C.* Rather than generating and storing a large number of gyro rate samples on tape, we instead compute the rates at each step of the Runge-Kutta integration and add Gaussian noise to the true values, to simulate gyro and A/D conversion errors.

Although our "truth model" for Process C is not sophisticated, we

*The linkup of Processes B and C can be implemented within the same microcomputer or using parallel microcomputers. We will address this issue in the Phase III effort.

nevertheless believe it is satisfactory for testing the validity of Process C. The reason for this belief is that, in a steady state mode, the integrated state will usually be much more poorly determined than the "fresh" data from Process B. Thus, the optimal, up-dated state output from Process C will nearly equal the Process B output data. This is borne out by our simulations.

5.0 SIMULATIONS

5.1 Process B

The functions of Process B are outlined in Figure 5.1. Presently, input data for FOV(A) is read from tape; this consists of estimated orientation parameters, number of stars in each FOV and a list of image plane coordinates and intensities (magnitudes) for the measured stars. Given the orientation estimates, the star catalog is accessed to retrieve those stars which lie within some uncertainty border around the estimated boresight. Cosines of inter-star angles are computed for the measured stars and tabulated. We next begin a series of tests comparing cosines of inter-star angles for pairs of catalog stars with the table of measured values and look for a match. This pairing begins with stars nearest the estimated boresight and proceeds outward until a match is obtained. Refer to the Phase I report for more details.

Once a match has been obtained we perform a least-squares differential correction to correct the assumed orientation parameters until the mathematical projection of identified catalog stars onto the image plane overlays the measured stars in a least-squares sense. At this point, the subset of stars from the catalog is searched for additional confirming stars (i.e., stars that project onto the image plane near to a measured star). Stellar aberration effects are added to the catalog stars and a final least-squares correction is performed with up to 5 stars. The above process is repeated for FOV(B) in like manner. If we assume the interlock angles between FOV(A) and (B) are fixed or slowly varying, it is possible to estimate the orientation to within 5 arc seconds for the errors assumed in the image coordinates ($\sigma \sim 3.4\mu$).

Figure 5.1: OUTLINE OF PROCESS B FUNCTIONS

FOV(A)

- Read data from buffers:
  - measured coordinates from Process A
  - orientation estimates from Process C
- Compute (3x3) rotation matrix
- Obtain estimated boresight vector from last row of rotation matrix
- Access the star catalog for stars surrounding the boresight (a sub-catalog)
- For measured stars:
  - calculate cosine of interstar angle between each star pair
  - store cosine values and star pair indicator in a table
- For sub-catalog stars:
  - calculate cosine between star pairs
  - compare each cosine with the table of measured cosines
  - test for a match (if no match, restart)
- Perform iterative least-squares differential correcton:
  - calculate the matrix of derivatives, (A), consisting of partials of stellar colinearity equations with respect to the orientation parameters, evaluated for the two paired stars
  - calculate residuals (ΔY) between measured coordinates and coordinates for the two catalog stars projected on the image plane
  - compute corrections to orientation parameters: $\Delta\beta = (A^T WA)^{-1} A^T W\Delta Y$ where W is a weight matrix
  - add corrections to current values $\beta_{k+1} = \beta_k + \Delta\beta$
  - test for small corrections; repeat if necessary
- Search for confirming star images:
  - compute image coordinates for all stars in sub-catalog
  - compare coordinates of each catalog star with coordinates of each measured star

- save measured and catalogued pair if close
- if there are no new pairs beyond the original pair, reject orientation and continue cosine pairing to look for another pair match
- repeat least-squares with up to 5 stars

FOV(B)

- Read data from buffer:
  - measured coordinates from Process A
  - use orientation from FOV(A) solution
- Repeat same steps as for FOV(A) for pairing stars and least-squares correction

Combined Solution:

- compute or obtain interlock angles between FOV(A) and FOV(B)
- compute derivative matrix (A) for up to 5 stars from each FOV
- compute coordinate deviations (ΔY) for these stars
- compute correction to orientation parameters:

  $$\Delta\beta = (A^T W A)^{-1} A^T W \Delta Y$$

- add corrections and test for smallness; repeat if necessary

Output:

- Output to buffer:
  - orientation parameters
  - covariance matrix for orientation parameters
  - associated time

One goal of the Process B simulations was to measure the average solution time for a set of data from Process A. Our present software, written in high-speed interpreter BASIC, can process a set of measurements in about 30 seconds of real time. This figure includes tape and disk read time (approximately 5 sec.). The total of 30 seconds is certainly an upper limit for a flight system.

A more important goal of Process B simulation is to measure the orientation accuracy relative to input errors. Simulations discussed here involved Rodrigues parameters which do not yield a readily interpretable result for error analysis. Therefore, two angles were computed which give a clearer measure of errors. Since the true orientation is known, we can compute the angular error in boresight direction by computing the cross product between the true and the calculated boresights.

This angle is then used to rotate the calculated frame into the true frame, so that the boresights coincide. Then the rotation about the true boresight is calculated, again by using a cross product. Refer to Appendix C for a complete discussion of this procedure. The two angles measure the angular error off the true boresight and the angular rotation error about the true boresight. The results of several typical successive trials are listed in Table 5.1. It appears from this table that 5-10 arc second accuracy is obtainable for the assumed geometry and system parameters. As will be discussed more fully in Section 6, the assumed error of 3.4μ (or 1/10 of a pixel) for the image coordinates is probably an upper limit and may be reduced to 5% pixel or less by various means. Also, the error is proportional to scale factor, i.e., attitude error is inversely proportional to the lens focal length (and field size).

Trial	Number of Stars in FOV		Error of Principal Line	Error of Principal Rotation	Error of FOV(A):	
					Boresight Direction	Rotation about True Boresight
	(A)	(B)	$\Delta\ell$(arcsec)	$\Delta\Phi$(arcsec)	(arcsec)	(arcsec)
1	5	5	3.76	3.22	4.78	6.38
2	4	5	0.51	6.87	8.82	9.97
3	4	3	8.63	8.09	13.59	7.60
4	5	4	2.86	3.03	5.05	5.08
5	3	4	0.58	2.53	3.35	4.42
6	5	2	8.09	3.95	7.77	10.88
7	5	4	4.66	0.60	1.93	3.60
8	4	3	7.84	6.24	8.52	4.99
9	5	4	2.98	3.31	5.37	4.92
10	5	4	4.83	1.30	3.57	5.27
11	5	5	6.04	1.67	5.44	4.42

Table 5.1. Orientation errors of 11 successive trials of Process B using two fields of view and fixed interlock angels.

5.2 Process C Simulations

The software for Process C is more straightforward than that of Process B. Process C is functioning presently with Rodrigues parameters. The state vector, then, contains six elements: 3 orientation parameters and 3 rate gyro bias values. A typical simulation result is shown in Figure 5-2. To test Process C we have generated simulated output from Process B consisting of three Rodrigues parameters and associated covariance matrix for each time step of 30 seconds. Any initial set of three Rodrigues parameters is suitable for testing Process C. However, generating a realistic covariance matrix associated with that set and subsequent sets is difficult. This is due, in part, to the infinite range of Rodrigues parameters which causes a wide range of values for the covariance matrix. Also, errors in orienting the FOV are not easily mapped into errors in the Rodrigues parameters and the covariance matrix. We have not generated rigorous covariance matrices, since the present software is considered a "stepping-stone" toward the Euler parameter-based software. Therefore, Figure 5-2 should be viewed as illustrating the general behavior of the Kalman filter in response to data from Process B and to the state obtained from integrating the rate gyro data.

The vertical scale of Figure 5-2 is in arc-seconds, approximately transformed from the Rodrigues parameters output from the Kalman filter. We have also included (Figure 5-3) Phase I results of Kalman filter simulations using Euler angle data. From a comparison of Figure 5-2 and 5-3 one can easily see the similar behavior for the Kalman filter processing of either Euler angle or Rodrigues parameter data.

Our simulations have shown that, after a steady state has been reached, the updated orientation parameters output from the Kalman filter are nearly equal to the parameters output by Process B. The near equality is due to the significantly smaller covariance associated with the Process B parameters as compared to the covariance associated with the orientation parameters obtained by forward integration of the kinematic differential equations using rate gyro data. However, we find that the gyro bias estimates obtained from Process C oscillate about their true value on a short time scale and with a deviation similar to the gyro noise value (refer to Table 5.2 and Figure 5.2). This oscillation appears to be due primarily to the similar magnitudes of the gyro biases and assumed gyro noise. Thus, gyro noise is "interpreted" by the Kalman filter as a change in the gyro biases even though the true biases, in these simulations, are constant. We suggest smoothing the raw gyro rates (by averaging multiple values, for example), since the gyro readout rate is much higher than required by the Runge-Kutta integration. Alternatively, the updated bias values can be averaged into a running average (an average of, say, the last 50 values). Application of either or both of these methods would smooth the recovered bias values sufficiently so that we can monitor long term bias changes. These methods have been applied for short series of runs. During Phase III we will perform more extensive tests.

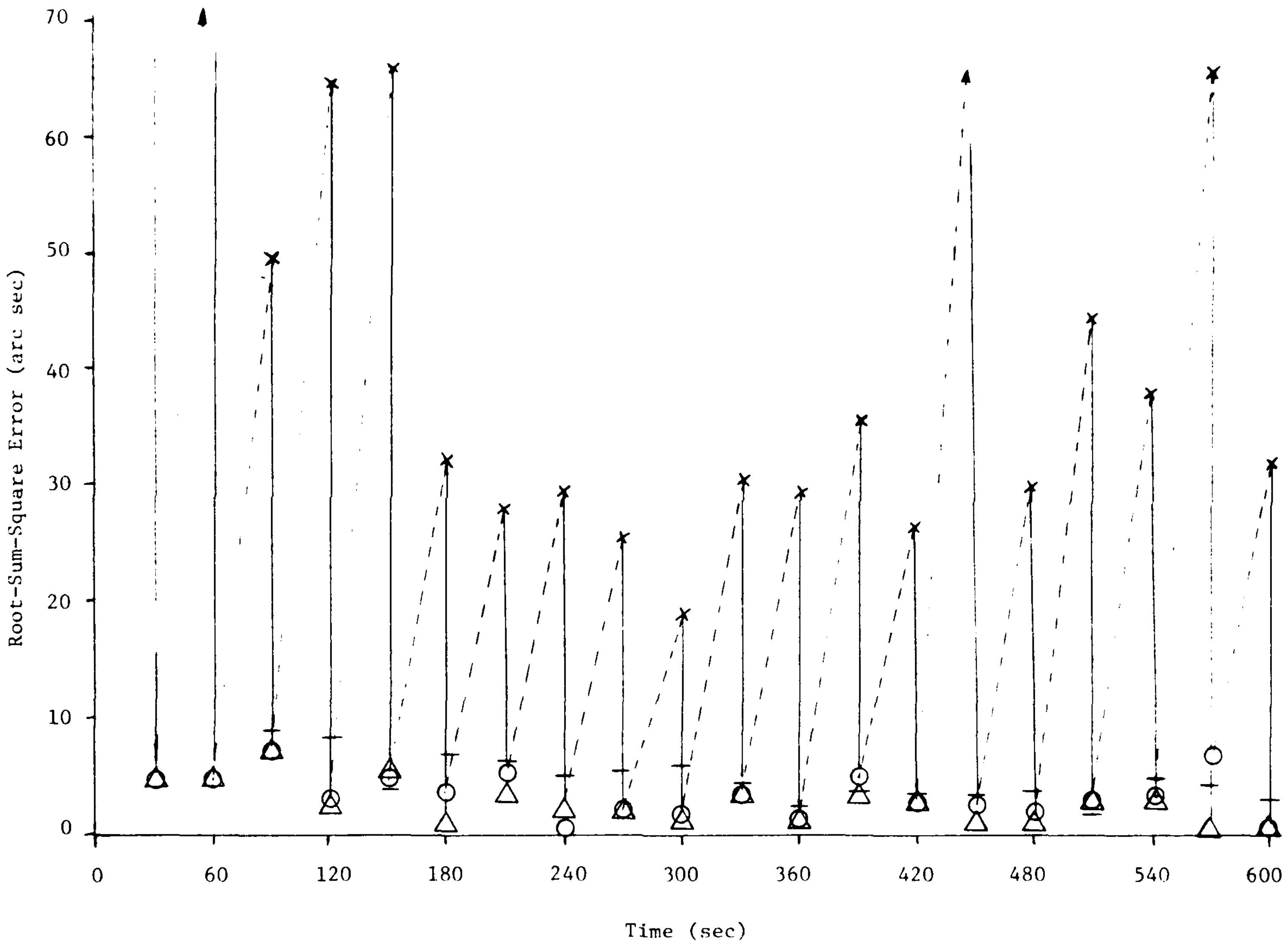

Figure 5.2. Process C simulation results using Rodrigues parameters for 30 second intervals. (x = Orientation error after forward integration, Λ = orientation error of Process B output, 0 = orientation error of optimal estimate, — = estimated error as given by covariance matrix)

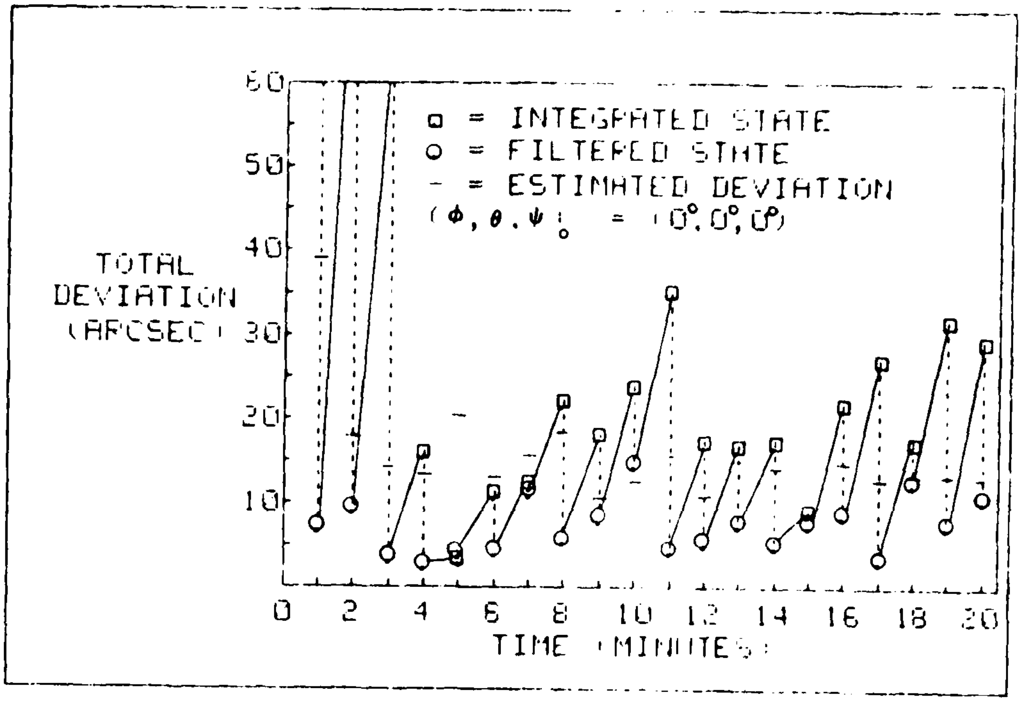

Figure 5.3a Kalman filter results for Process C simulation: Case I

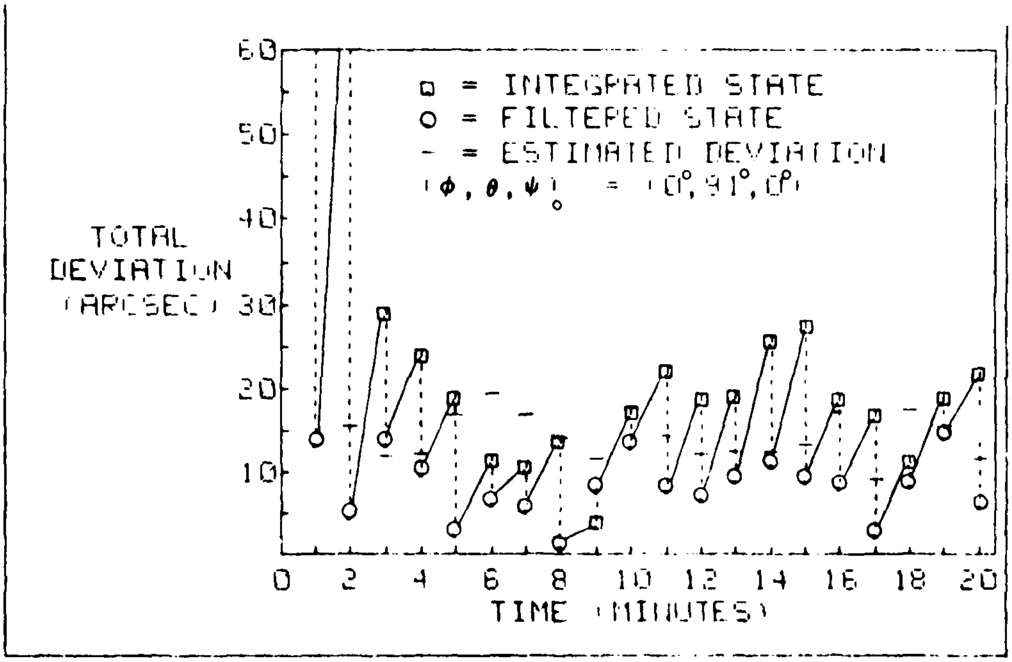

Figure 5.3b Kalman filter results for Process C simulation: Case II

Table 5.2 Recovered bias values for 10 min series. Initial estimates were 0.

time(sec)	b_1	b_2	b_3
30	5.761E-6	8.822E-6	6.694E-6
60	5.220	7.076	4.816
90	6.635	2.755	3.025
120	6.540	3.802	4.965
150	4.769	-0.739	5.057
180	5.412	2.053	4.646
210	5.449	2.991	4.180
240	5.761	4.873	3.723
270	5.935	5.200	3.634
300	6.000	5.311	3.597
330	5.626	5.285	3.734
360	5.335	4.935	4.406
390	5.098	4.424	4.752
420	4.691	3.959	4.904
450	4.742	3.775	4.881
480	4.751	3.752	5.012
510	5.008	3.798	5.357
540	4.921	3.913	5.127
570	5.018	4.086	5.442
600	5.109	4.219	5.408
Average	5.389	4.215	5.151
True Value	4.848E-6	4.848E-6	4.848E-6

6.0 CONCLUSIONS OF PHASE II RESEARCH

We have met several research objectives through the efforts during Phase II. The research has also suggested new directions for future refinements and improvements.

Our simulations of Process B have focused on "steady-state" operation. That is, simulations in which the estimated orientations were not in error by a large amount and there were at least several stars in each FOV. In nearly all steady-state examples the solution time was 30 seconds or less of real time, including about 5 seconds required for reading input data from tape and for accessing the star catalogue stored on disk. The solution time for Process B, as it is currently configured, is an upper limit and can be shortened considerably. There are several factors leading to a decrease.

We note that memory-to-memory data transfers are significantly faster than memory-to-storage device transfers. Therefore, a flight computer system, employing memory buffers for data transfers between subsystems and a memory bank for the star catalog, would save at least five seconds over the present system over and above savings which may be realized as a result of the particular flight computer doing arithmetic faster than the HP9845A.

A more significant time savings can be realized by programming Process B in microcode or by using a compiled program form. The present computer system uses a high-speed BASIC interpreter; i.e., each line of BASIC code must be translated or interpreted and then executed. A factor of five increase in speed may be possible with a microcode program. On the basis of our simulations and the above comments, we conclude that Process B can <u>easily</u> be carried out within the constraints of on-board computations. We note that Process B (as refined during Phase III) will have some additional logic and this will lengthen the program slightly. The bulk of the computations are being performed in the present version, however.

We are also near our accuracy goal of 5-10 arcseconds using an adopted system and associated parameters when there are 4-5 stars per FOV. Before we can unequivocally make this claim for accuracy, we must be sure we are accurately modeling Process A output data (star image centroids). We emphasize that the accuracy of the Process B output data depends directly on the quality of Process A output data. Thus, any accuracy claim for Process B must be accompanied by figures for the accuracy of Process A (and type of star tracker). The 5-10 arcseconds goal can, no doubt, be exceeded by redesigning the system around a longer focal length lens and admitting fainter stars. However, the storage and manipulation of the resulting increased population of visible stars, may be beyond the capabilities of a real-time on-board system.

Process C has not been tested as extensively as has Process B. However, our simulations of Process C show that it satisfies the time constraints of on-board computation. Process C is extremely fast -- typically 5 seconds for the Runge-Kutta integration and Kalman filter update sections combined. The decrease in solution time by using a microcode version will not be as dramatic as for Process B. Much of the current software makes extensive use of the BASIC matrix commands of the HP9845A (such as matrix multiplication and matrix inversion), each of which is already in machine language and therefore very fast. However, we expect some savings by converting to Euler parameters and using the associated, more efficient, relationships for computing the state transition matrix.

7.0 OUTLOOK FOR PHASE III RESEARCH

Phase III research will focus primarily on extensive testing and integration of the complete attitude system. We will continue to study new approaches and new techniques as well.

Our first task will be the conversion from Rodrigues parameters to Euler parameters, as outlined in Section 2.1. This task should be straightforward since most of the calculations and logic have been formulated. Software conversion has begun.

A second significant task is the editing and transfer of the SKYMAP star catalog to the HP9845 system. The catalog will be stored on disk in place of the present simulated catalog. The SKYMAP catalog, currently stored on the IBM 370/158 computer, may be modified prior to transfer. No attempt was made originally to have the catalog uniform in number of stars per cell. We simply selected the 5000 brightest stars. However, for accurate attitude determination we may desire at least 5 detectable stars per FOV. Near the galactic pole we will need a fainter limiting magnitude in order to obtain this number compared to the galactic equator regions. To maximize the overlap between the observed stars and catalogued stars, the integration time of the CCD sensor must be variable and/or Process A logic structured to select and process images from the 5 or 6 brightest stars in any field.

We must also delete double stars from the catalog. This includes all star pairs with separations less than the resolution of the CCD sensor. We have postponed this task until we have a firmer resolution value for a typical CCD star sensor.

Further refinements will be added to Process B. We must add calculations and logic to monitor the FOV interlock angles. A third FOV should be added, at least for general use, so that any pair of sensors could be used for attitude determination. A third sensor would provide a backup should one sensor fail and permit a small sun angle for one sensor, leaving two others operational for accurate attitude determination.

Appropriate "start-up" logic must be incorporated into Process B; this logic decides whether to continue searching for a star pair match or to reject Process A data and request a new set. We are presently studying techniques with which to re-access the star catalog should Process B fail to find a star pair match near the estimated boresight. Our current thoughts are to access, in succession, five or six adjacent FOV-size star subsets located around the original estimated FOV. Each star subset would be treated in the same manner as the subset containing the original estimated FOV. The software for this scheme has been written but not yet incorporated into the existing Process B code.

As our final task, we propose to run extensive simulation tests of Processes B and C. To do this, we will first simulate as accurately as possible the data from Process A. As mentioned before, some of the error sources can be corrected for in Process A. There will be errors in positions due to random noise inherent in the CCD and associated electronics and noise due to response variations from pixel to pixel. Errors of this nature depend on the type of CCD and electronic design used. They are presently modeled as errors in star position which belong to Gaussian distributions. The accuracy results of Process B and C simulations will then be proportional to the selected standard deviation. We will assume that systematic errors in the star sensors can be removed by apriori and dynamic calibrations applied in Process A.

The simulated data from Process A will represent data frames separated by perhaps 30 seconds of time and for several fractional orbits of a typical satellite. Tests will determine 1) the rate of failure for Process B to determine any attitude and 2) the accuracy of the solutions for attitude as a function of number of stars, possibly the placement of the stars in the field, and magnitudes of the stars. By randomly pointing the boresight axes we can also test the "start-up" capability of Process B relative to initial estimates.

Process C tests will determine the ability of the Kalman filter to produce an optimal estimate near the true state vector in the steady state mode. Finally, the speed of Process B and C will be measured.

We shall also determine whether Processes B and C actually need to be run in parallel or if they can function adequately in a sequential fashion. If a parallel mode is desirable, we will configure a parallel test/demonstration of Processes B and C.

8.0 REFERENCES

1. Junkins, J. L., Optimal Estimation of Dynamical Systems, Sijthoff-Noordhoff International Publishers, The Netherlands, 1978, pg. 154.

2. Junkins, J. L., Strikwerda, T. E., and Kraige, L. G., Star Pattern Recognition and Spacecraft Attitude Determination, Phase I, VPI&SU Report No. VPI-E-79.4, VPI&SU, Blacksburg, VA 24061.

APPENDIX A: STAR CATALOG FORMAT

As of this writing we have not transfered the SKYMAP star catalog from the IBM 370/158 computer to the HP9845. To procede with testing and to gain experience with the form for the catalog, a pseudo-catalog was created on the HP9845. This was generated by computing 5000 random star positions, from a uniform distribution over the celestial sphere, and computing star magnitudes. The stars were then reordered into cells using the techniques described in the Phase I report. After some thought, it was decided to have 529 cells (22 latitude bands of equal width). Choice of this number was influenced, in part, by the FOV size of 7° x 9° adopted for these simulations. With this field size, the catalog access routine reads data from the 4 nearest neighboring cells around the estimated boresight (Figure A.1) and thus provides nearly complete coverage of the estimated FOV by the 4 cells.

To facilitate computer access, the catalog was stored on disk in a direct access format. Preceeding the catalog proper is a table containing the position in the file of each cell and the number of stars in each. Thus, each cell can be accessed rapidly and independently.

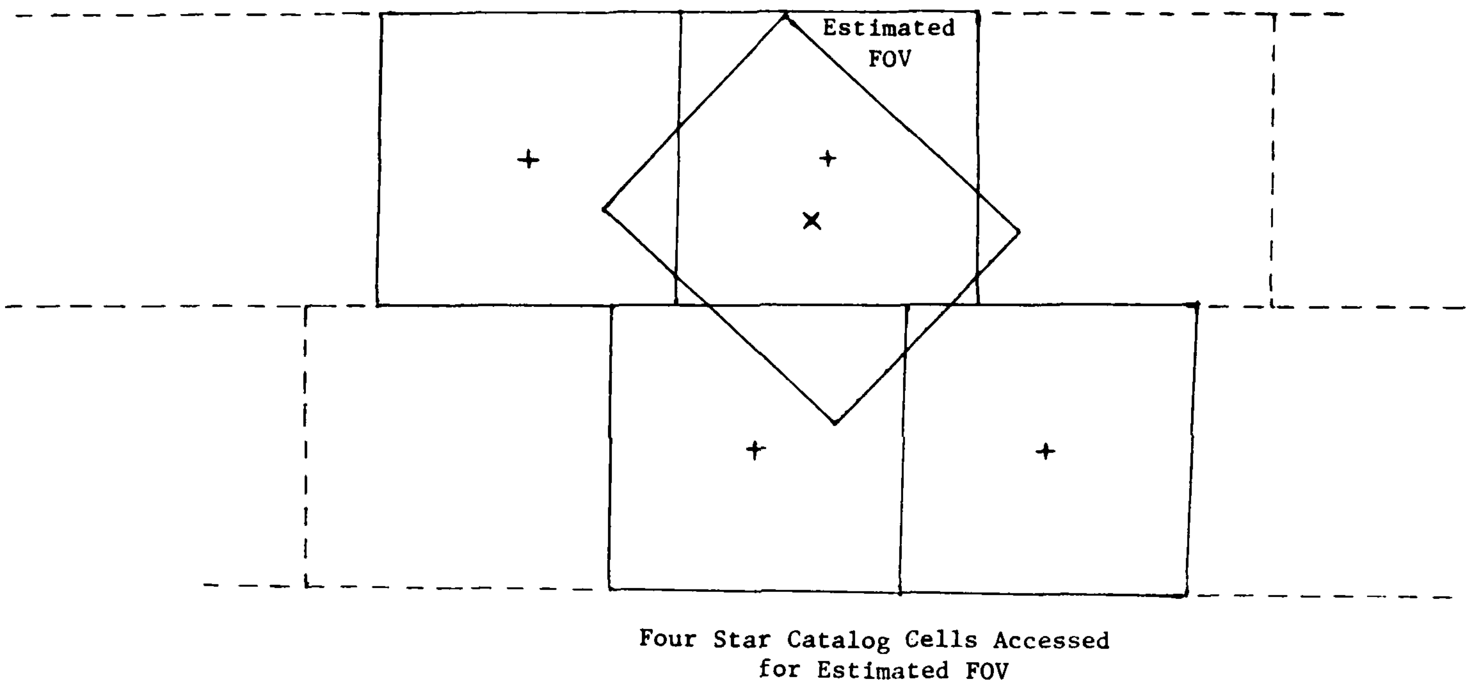

Figure A.1. Catalog cell pattern obtained for a typical estimated field of view.

APPENDIX B: STELLAR ABERRATION

The effect of stellar aberration is to cause a star's apparent direction to shift towards the direction of the observers motion. The amount of shift depends on both the velocity of the observer and on the angle between the observer's line of sight (the star direction) and the velocity vector. The shift is:

$$a = \frac{v}{c} \sin \alpha \qquad \text{(B.1)}$$

where a = aberration in radians

v = observer's speed

c = velocity of light

α = angle between velocity vector and the true star direction.

For our purpose, we must express a star's shifted direction in terms of the true direction, the vehicle velocity and the angle between the velocity vector and true direction; that is,

$$\begin{Bmatrix} L_x' \\ L_y' \\ L_z' \end{Bmatrix} = f(L_x, L_y, L_z, v, \alpha) \qquad \text{(B.2)}$$

If we let $\underline{v}_s$ be the velocity of starlight in the inertial frame and $\underline{v}$ be observer velocity, then the relative velocity of the starlight as seen by the observer is:

$$\underline{v}_{s/o} = \underline{v}_s - \underline{v} \qquad \text{(B.3)}$$

Now, if we let $\hat{\underline{\ell}}_n$ be the unit vector in the true direction and $\hat{\underline{\ell}}_n'$ the unit vector in the shifted direction, we can rewrite this as (refer to Figure B1)

$$(c + v \cos \alpha)\ \hat{\underline{\ell}}_n' \cong c\hat{\underline{\ell}}_n + \underline{v} \qquad \text{(B.4)}$$

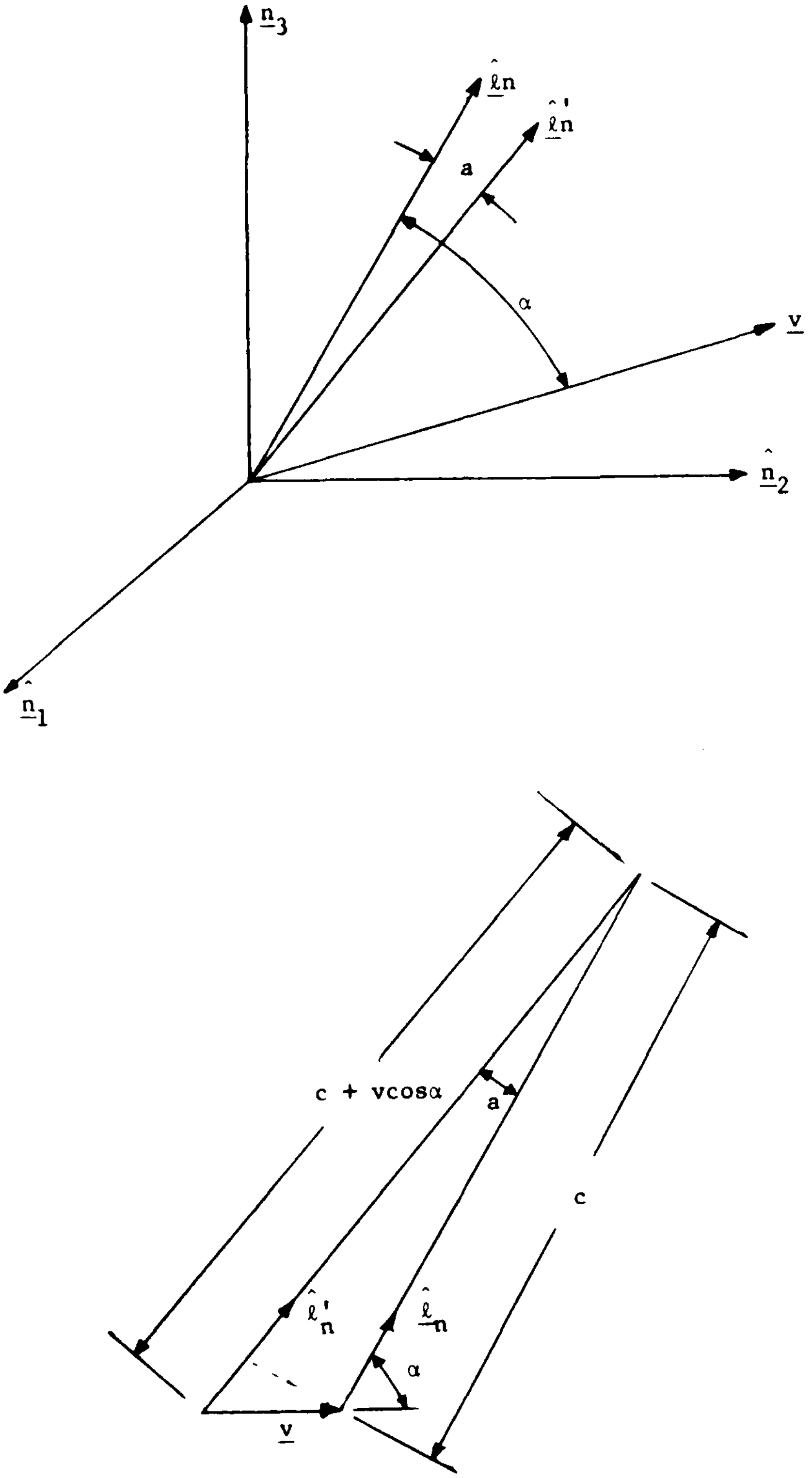

Figure B.1. Star direction displacement of stellar aberration due to observer's velocity.

To first order this becomes

$$\hat{\underline{\ell}}'_n = (1 - \frac{v}{c}\cos\alpha)\hat{\underline{\ell}}_n + \frac{\underline{v}}{c} \qquad \text{(B.5)}$$

or

$$\begin{Bmatrix} L'_x \\ L'_y \\ L'_z \end{Bmatrix} = (1 - \frac{v}{c}\cos\alpha)\begin{Bmatrix} L_x \\ L_y \\ L_z \end{Bmatrix} + \frac{1}{c}\begin{Bmatrix} v_x \\ v_y \\ v_z \end{Bmatrix} \qquad \text{(B.6)}$$

This equation is used for calculating the displacement of a star's unit vector. The velocity vector is computed for the combined velocity of the earth and satellite and Herrick's "f and g" solution is used to calculate the individual velocities each time Process B accepts new data from Process A.

We note several points concerning the effects of aberration on the star tracker. The speed of the earth in its orbit is 30 km/s and the maximum speed of an earth orbiting satellite is 8 km/s relative to the earth. Therefore, the maximum shift in a star's direction is about 26 arcseconds. This maximum occurs for stars 90° from the velocity vector. However, all stars in this neighborhood will be shifted by nearly this amount and, thus, the distortion of the FOV will be insignificant. However, aberration will displace the boresight direction. To avoid orientation errors in the combined FOV(A) and FOV(B) solution we must correct the catalogue direction cosines by applying equation (B.6).

For those stars in the direction of the velocity vector, the shift in direction will be small. But since the shift is always towards the velocity vector the distortion is noticeable (an apparent shrinking of the FOV). In this case, the aberration should be applied before the final least-squares solution for the single FOV.

APPENDIX C: CALCULATION OF ORIENTATION ERRORS

We have used Euler parameters or Rodrigues parameters to describe the orientation of the field of view (FOV) with respect to an inertial frame. For our simulation studies we can compare the calculated set of parameters with the true set. However, this comparison does not reveal the effect the errors have on the FOV orientation. Therefore, we define two angles, ε and μ, which are, respectively, the angular error in the calculated boresight direction and the rotation error about the true boresight between the calculated and true FOV.

For our calculation we consider only FOV(A). Consider two reference frames $\{\hat{a}_T\}$ and $\{\hat{a}_c\}$ which are the true and calculated frames for FOV(A) (refer to Figure C-1). The magnitude of the cross product between $\hat{a}_{3_c}$ and $\hat{a}_{3_T}$, the boresight vectors, yields the error ε, the angle between boresights:

$$\left|\hat{a}_{c_3} \times \hat{a}_{T_3}\right| = \sin\varepsilon \simeq \varepsilon.$$

The calculations for angle μ is more involved. We first define a new frame $\{\hat{c}\}$ such that

$$\hat{c}_1 = \hat{a}_{c_3}$$

$$\hat{c}_2 = \hat{c}_3 \times \hat{c}_1$$

$$\hat{c}_3 = (\hat{a}_{c_3} \times \hat{a}_{T_3})/\sin\varepsilon.$$

From this we can determine the rotation matrix [CN]. The unit vector, $\hat{a}_{c_1}$, is rotated into the $\{\hat{c}\}$ frame:

$$\hat{d} \equiv [CN]\hat{a}_{c_1}.$$

This unit vector is rotated by the angle ε about $\hat{c}_3$ in the $\{\hat{c}\}$ frame:

$$\hat{r} \equiv [R(\varepsilon)]\hat{d}.$$

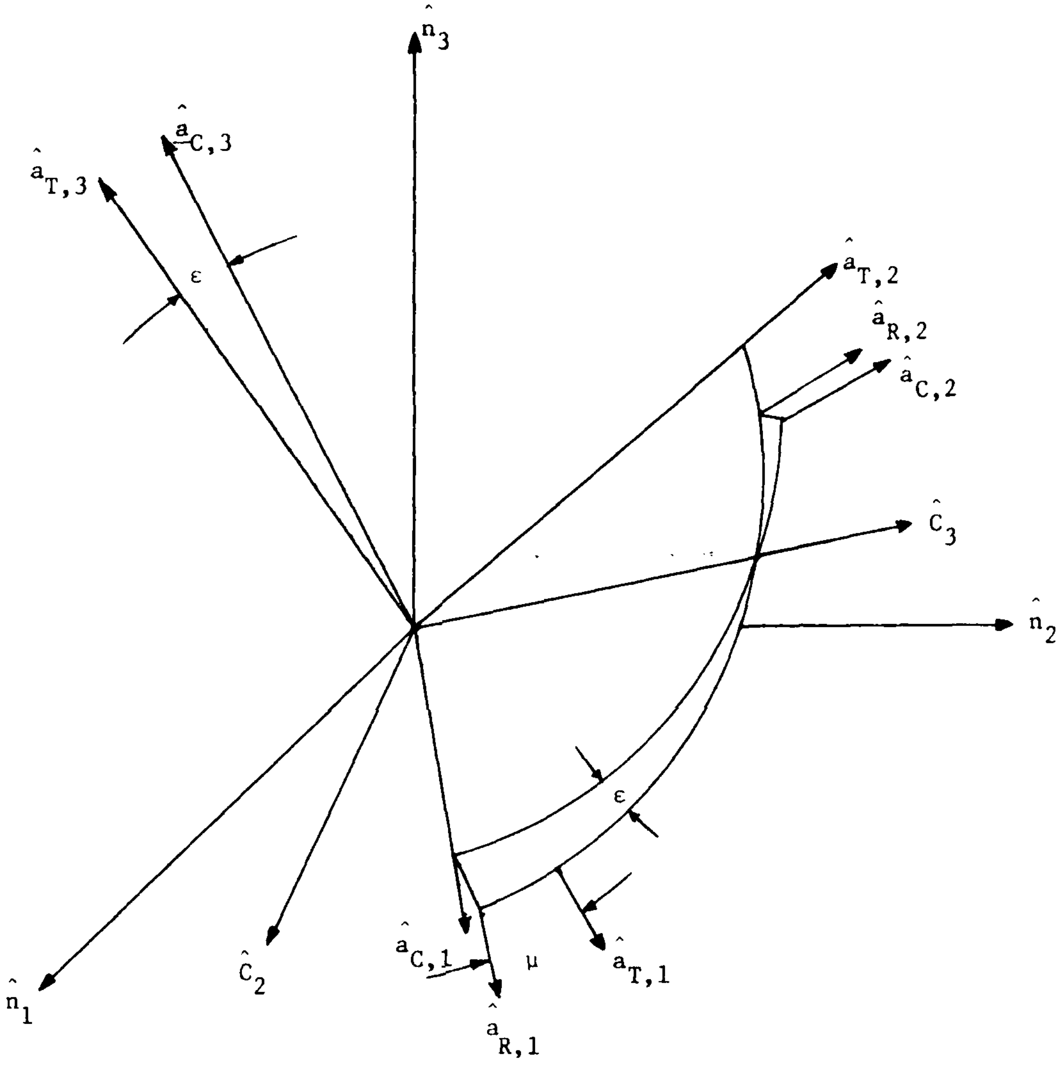

$$\hat{C}_1 = \hat{a}_{C,3}$$

$$\hat{C}_2 = \hat{C}_3 \times \hat{C}_1$$

$$\hat{C}_3 = (\hat{a}_{C,3} \times \hat{a}_{T,3})/\sin \varepsilon$$

Figure C.1. Coordinate frames needed for computing angular errors between the true and calculated fields of view.

$$\text{where } [R(\varepsilon)] = \begin{bmatrix} \cos \varepsilon & \sin \varepsilon & 0 \\ -\sin \varepsilon & \cos \varepsilon & 0 \\ 0 & 0 & 1 \end{bmatrix}.$$

Finally, this unit vector, $\hat{r}$, is rotated back into the inertial frame:

$$\hat{a}_R \equiv [CN]^T \hat{r}$$

Combining these equations we write:

$$\hat{a}_R = [CN]^T [R(\varepsilon)][CN]\hat{a}_{c_1}.$$

To calculate the rotation about the true boresight we compute:

$$\left| \hat{a}_R \times \hat{a}_{T_1} \right| = \sin \mu \simeq \mu$$

These two angles, ε and μ, give a good pointing error measure for the star tracker system.

Unclassified
SECURITY CLASSIFICATION OF THIS PAGE (When Data Entered)

19 REPORT DOCUMENTATION PAGE

READ INSTRUCTIONS
BEFORE COMPLETING FORM

1. REPORT NUMBER
18 ETL-0211

2. GOVT ACCESSION NO.
AD-A090195

3. RECIPIENT'S CATALOG NUMBER

4. TITLE (and Subtitle)
6 STAR PATTERN RECOGNITION AND SPACECRAFT ATTITUDE DETERMINATION. ~~PHASE~~

5. TYPE OF REPORT & PERIOD COVERED
9 Interim ~~Contract~~ Report, 1 Oct 78- 30 Sep 79 on phase

6. PERFORMING ORG. REPORT NUMBER

7. AUTHOR(s)
10 Thomas E. Strikwerda
John L. Junkins

8. CONTRACT OR GRANT NUMBER(s)
15 DAAK70-78-C-0038

9. PERFORMING ORGANIZATION NAME AND ADDRESS
Engineering Science and Mechanics Dept.
Virginia Polytechnic Institute and State Univ.
Blacksburg, VA 24061

10. PROGRAM ELEMENT, PROJECT, TASK AREA & WORK UNIT NUMBERS

11. CONTROLLING OFFICE NAME AND ADDRESS
U.S. Army Engineer Topographic Laboratories
Fort Belvoir, Virginia 22060

12. REPORT DATE
11 Dec~~ember 1~~979

13. NUMBER OF PAGES

14. MONITORING AGENCY NAME & ADDRESS (if different from Controlling Office)
12 58

15. SECURITY CLASS. (of this report)
Unclassified

15a. DECLASSIFICATION/DOWNGRADING SCHEDULE

16. DISTRIBUTION STATEMENT (of this Report)
Distribution unlimited

17. DISTRIBUTION STATEMENT (of the abstract entered in Block 20, if different from Report)

18. SUPPLEMENTARY NOTES

19. KEY WORDS (Continue on reverse side if necessary and identify by block number)
spacecraft, pointing, attitude, CCD, triangulation, control

20. ABSTRACT (Continue on reverse side if necessary and identify by block number)

Interim results (Phase II) are reported from a research and development project concerned with exploitation of CCD matrix detectors in a new generation of autonomous, real-time star sensing, identification, and spacecraft attitude determination. The results reported include the following:

(1) Continued development of an approach for real-time, on-board estimation of spacecraft attitude with sub-

Unclassified
SECURITY CLASSIFICATION OF THIS PAGE (When Data Entered)

404722

Block 20 - five arc-second precision.

(2) Implementation and validation of several variations of the approach in a laboratory microcomputer - the objective being to ascess the problems associated with a real-time, on-board version of this system.

(3) Development of truth models to generate realistic input data for the star pattern recognition and Kalman filter strategies.

(4) Conversion from use of Euler angles to Rodrigues parameters to define vehicle attitude, affecting the algorithms for star-pattern recognition, least-squares differential correction to refine estimated attitude, and the Kalman filter strategy to obtain the optimal attitude estimate.

(5) Formulation of algorithms using Euler parameters to define orientation.

The phase III effort (in progress) will continue the above developments, culminating in extensive validation tests and documentation of the results.

FILME